of the estimated reactivity ratios.

As a final conclusion we have to stress the great potential of the free-radical copolymerization of easily available chiral monomers, such as (−)-menthyl acrylate and (−)-menthyl methacrylate, with *N*-vinylcarbazole to achieve synthetic macromolecules in which the heteroaromatic chromophores strongly contribute to the optical rotation of the polymer as a whole.

Acknowledgment. We are grateful to SRC (U.K.) and CNR (Italy) for financial support.

References and Notes

(1) Pino, P. *Adv. Polym. Sci.* **1965**, *4*, 393.
(2) Pino, P.; Ciardelli, F.; Zandomeneghi, M. *Annu. Rev. Phys. Chem.* **1970**, *21*, 561.
(3) Pino, P.; Salvadori, P.; Lorenzi, G. P.; Chiellini, E.; Lardicci, L.; Consiglio, G. B.; Bonsignori, O.; Lepri, L. *Chim. Ind. (Milan)* **1973**, *55*, 182.
(4) Pino, P.; Carlini, C.; Chiellini, E.; Ciardelli, F.; Salvadori, P. *J. Am. Chem. Soc.* **1968**, *90*, 5025.
(5) Ciardelli, F.; Salvadori, P.; Carlini, C.; Chiellini, E. *J. Am. Chem. Soc.* **1972**, *94*, 6536.
(6) Carlini, C.; Chiellini, E. *Makromol. Chem.* **1975**, *176*, 519.
(7) Ciardelli, F.; Salvadori, P.; Carlini, C.; Menicagli, R.; Lardicci, L. *Tetrahedron Lett.* **1975**, 1779.
(8) Ciardelli, F.; Carlini, C.; Chiellini, E.; Salvadori, P.; Lardicci, L.; Pieroni, O. "Proceedings of the 5th European Symposium on Polymer Spectroscopy"; Hummel, D. O., Ed.; Verlag Chemie GmbH: Weinheim, 1979; p 131.
(9) Ciardelli, F.; Chiellini, E.; Carlini, C.; Pieroni, O.; Salvadori, P.; Menicagli, R. *J. Polym. Sci., Polym. Symp.* **1978**, *No. 62*, 143.
(10) Chiellini, E.; Solaro, R.; Palmieri, M.; Ledwith, A. *Polymer* **1976**, *17*, 641.
(11) Chiellini, E.; Solaro, R.; Colella, O.; Ledwith, A. *Eur. Polym. J.* **1978**, *14*, 489.
(12) Chiellini, E.; Solaro, R.; Ledwith, A. *Makromol. Chem.* **1978**, *179*, 1929.
(13) Johnson, G. E. *J. Chem. Phys.* **1975**, *62*, 4697.
(14) Houben, J. L.; Natucci, B.; Solaro, R.; Colella, O.; Chiellini, E.; Ledwith, A. *Polymer* **1978**, *19*, 811.
(15) Read J.; Grubb, W. J. *J. Chem. Soc.* **1939**, 1156.
(16) Schulz, R. C.; Kaiser, F. *Makromol. Chem.* **1965**, *86*, 80.
(17) Frank, R. L.; Davis, H. R.; Drake, S. S.; Mc Pherson, J. B., Jr. *J. Am. Chem. Soc.* **1944**, *66*, 1509.
(18) Menchini, G. B. Thesis, University of Pisa, 1972.
(19) Lopatinskii, V. P.; Sirotkina, E. E.; Anusova, M. M.; Tikhonova, L. G.; Pavlov, S. F. *Izv. Tomsk. Politekh. Inst.* **1964**, *126*, 58 (*Chem. Abstr.* **1965**, *63*, 18007*h*).
(20) Majumdar, R. N.; Carlini, C. *Makromol. Chem.* **1980**, *181*, 201.
(21) Majumdar, R. N.; Carlini, C.; Rosato, N.; Houben, J. L. *Polymer* **1980**, *21*, 941.
(22) Vollmert, B. "Polymer Chemistry"; Springer-Verlag: New York, 1973; p 108.
(23) Mayo, F. R.; Walling, C. *Chem. Rev.* **1950**, *50*, 200.
(24) Schulz, R. C. *Z. Naturforsch.* **1964**, *193*, 387.
(25) Solaro, R.; Chiellini, E. *Gazz. Chim. Ital.* **1976**, *106*, 1037.
(26) Carlini, C.; Ciardelli, F.; Pino, P. *Makromol. Chem.* **1968**, *119*, 244.
(27) Chiellini, E.; Carlini, C. *Makromol. Chem.* **1977**, *178*, 2545.
(28) Okamoto, Y.; Suzuki, K.; Ohta, K.; Hatada, K.; Yuki, H. *J. Am. Chem. Soc.* **1979**, *101*, 4763.
(29) Yuki, H.; Ohta, K.; Okamoto, Y.; Hatada, K. *J. Polym. Sci., Polym. Lett. Ed.* **1977**, *15*, 589.
(30) Ohta, K.; Hatada, K.; Okamoto, Y.; Yuki, H. *J. Polym. Sci., Polym. Lett. Ed.* **1978**, *16*, 545.
(31) Bigelow, R. W.; Johnson, G. E. *J. Chem. Phys.* **1977**, *66*, 4861.
(32) Yoshikawa, M.; Nomori, H.; Hatano, M. *Makromol. Chem.* **1978**, *179*, 2397.
(33) Hatano, M.; Nomori, H.; Yoshikawa, M. "Proceedings of the 5th American Peptide Symposium"; Goodman, M., Meinhofer, J., Eds.; Wiley: New York, 1977; p 390.
(34) Chiellini, E.; Solaro, R.; Ciardelli, F.; Galli, G.; Ledwith, A. *Polym. Bull.* **1980**, *2*, 577.
(35) Chiellini, E.; Solaro, R.; Ledwith, A.; Galli, G. *Eur. Polym. J.* **1980**, *16*, 875.
(36) Chernobai, A. V.; Shepeleva, A. I.; Zubkova, V. S. *Vysokomol. Soedin.* **1965**, *7*, 1080.
(37) Ledwith, A.; Galli, G.; Chiellini, E.; Solaro, R. *Polym. Bull.* **1979**, *1*, 491.
(38) Williams, D. J. *Macromolecules* **1970**, *3*, 602.

Domain-Boundary Structure of Styrene–Isoprene Block Copolymer Films Cast from Solutions. 5. Molecular-Weight Dependence of Spherical Microdomains

Takeji Hashimoto,* Mineo Fujimura, and Hiromichi Kawai

Department of Polymer Chemistry, Faculty of Engineering, Kyoto University, Kyoto 606, Japan. *Received March 25, 1980*

ABSTRACT: A series of diblock polymers of polystyrene and polyisoprene having nearly equal polyisoprene content (about 15 wt %) but different total molecular weight were synthesized to study the domain size, interdomain distance, and the thickness of the domain-boundary interphase as a function of molecular weight for the spherical microdomain system in the solid state (polyisoprene spheres dispersed in a polystyrene matrix). Quantitative analyses with the small-angle X-ray scattering technique indicated that the size of the spherical domain (radius $\bar{R}$) and interdomain distance $\bar{D}$ vary, respectively, with the molecular weight of the polyisoprene block and that of the entire block polymer to the $^2/_3$ power, while the interfacial thickness is almost independent of the molecular weight covered in this work (about 1.8 nm). The $^2/_3$ power law is consistent with the results predicted from the equilibrium theory of Helfand and Wassermann but the absolute values of $\bar{R}$ and $\bar{D}$ are far below the theoretical values, due to a nonequilibrium effect encountered in the solvent evaporation process. Thus the spherical domain systems in the solid state are in a metastable state with an excess free energy attributed to an excess interfacial area or interfacial volume, which contrasts with the lamellar microdomain systems, where the systems are very close to the equilibrium state.

I. Introduction

In this series of papers[1-4] we have been exploring the microdomain structure and the structure of the polymer–polymer interphase in polystyrene–polyisoprene diblock polymers in relation to the fundamental molecular and thermodynamic variables of the systems by using the small-angle X-ray scattering (SAXS) technique. In part 1 we made a paracrystalline analysis for the block polymer having lamellar microdomains to investigate orientation of the domains, uniformity of the domain size and regularity in their spatial arrangement, and the thickness of the domain-boundary interphase where the incompatible

0024-9297/80/2213-1660$01.00/0

Table I
Domain and Domain-Boundary Properties of Spherical Microdomains

specimen	$10^{-4}M_n$ total	$10^{-4}M_n$ PI block	wt % PI block	domain $\bar{D}$, nm	domain $\bar{R}$, nm	domain $\sigma_r/\bar{R}$	domain boundary ΔR, nm	domain boundary $\Delta R/\bar{R}$	domain boundary f	domain boundary S/N, nm²
SI-1	8.0	1.3	16.0	24.2	6.6	0.15	2.0	0.30	0.21	10.6
SI-2	14.5	2.0	13.9	30.3	8.0	0.15	1.7	0.21	0.12	13.5
SI-3	20.2	2.6	12.9	35.3	9.4	0.11	1.7	0.18	0.094	14.9
SI-4	21.9	3.4	15.4	40.1	12.7	0.09	2.1	0.17	0.099	14.4
SI-5	32.2	7.1	21.9	64.0	17.1	0.10	2.0	0.13	0.092	22.3
SI-6	65.7	14.4	21.9	106.0	31.0	0.10	1.5	0.05	0.036	25.0

segments intermix.[1] The domain-boundary structure was more quantitatively studied in part 2[2] for the lamellar microdomains based on an analysis of the SAXS curve in the Porod-law region.[5] The estimated interfacial thickness and the domain size were shown to agree with values predicted from equilibrium theories[6,7] based on statistical mechanics of random-flight chains in the confined "domain space".

In part 4 we further studied the domain size and the interfacial thickness as a function of molecular weight for a series of block polymers having lamellar microdomains.[4] Quantitative analyses with the SAXS technique indicated that the interfacial thickness is almost independent of the molecular weight of the block polymers covered in the studies. The domain size was shown to vary with molecular weight to the $^2/_3$ power, in agreement with results predicted from equilibrium theories. The lamellar domain systems turned out to be very close to the equilibrium state, its characteristic structural parameters being predictable from molecular parameters such as the statistical segment lengths, segment densities, molecular weight of each block chain, and interaction parameter between the two block chains. It was concluded that the global conformation of chain molecules in the domain space can be described in terms of the random-flight chain statistics in the confined space under the constraint of uniform filling of space.[8,9] The statistical mechanical approach gives insights on the molecular conformation and packing in the domain space:[4] (i) the chain has a conformation fairly extended along the direction normal to the boundary, the root-mean-square end-to-end dimensions projected parallel ($\langle R_z^2\rangle^{1/2}$) and perpendicular to the boundary normal ($\langle R_x^2\rangle^{1/2} = \langle R_y^2\rangle^{1/2}$) having a ratio of 1.7:1, and (ii) the nearest-neighbor distance between the two chemical junction points in the interphase (~2.6 nm) is much smaller than $\langle R_x^2\rangle^{1/2} = \langle R_y^2\rangle^{1/2}$ (≃9.6 nm) (the values in parentheses being obtained for a particular block polymer), thus resulting in a heavy overlap of neighboring molecules in the domain.

In this paper we extend the studies described above for the lamellar domain system to the spherical domain system. This work is also considered to be an extension of our preliminary analyses on the spherical microdomains based on the smeared SAXS data (part 3).[3] We shall analyze the structural parameters for the spherical microdomain system as a function of molecular weight of the block polymers on the basis of the rigorous analysis of SAXS data as partially described by Todo, Hashimoto, and Kawai[10] for a particular spherical domain system, SI-3.

II. Experimental Section

1. Test Specimens. A series of styrene and isoprene diblock polymers were synthesized by anionic polymerization with *sec*-BuLi as an initiator and tetrahydrofuran as a polymerization medium. All samples were polymerized by sequentially polymerizing styrene monomers and then isoprene monomers. Table I includes some results of characterization, number-average total molecular weight measured by a high-speed membrane osmometer, and weight fraction of polyisoprene block chain determined from elemental analysis. The microstructure of polyisoprene prepared in tetrahydrofuran medium contains 38, 59, and 3% 1,2-, 3,4-, and 1,4-additions, as described elsewhere.[11]

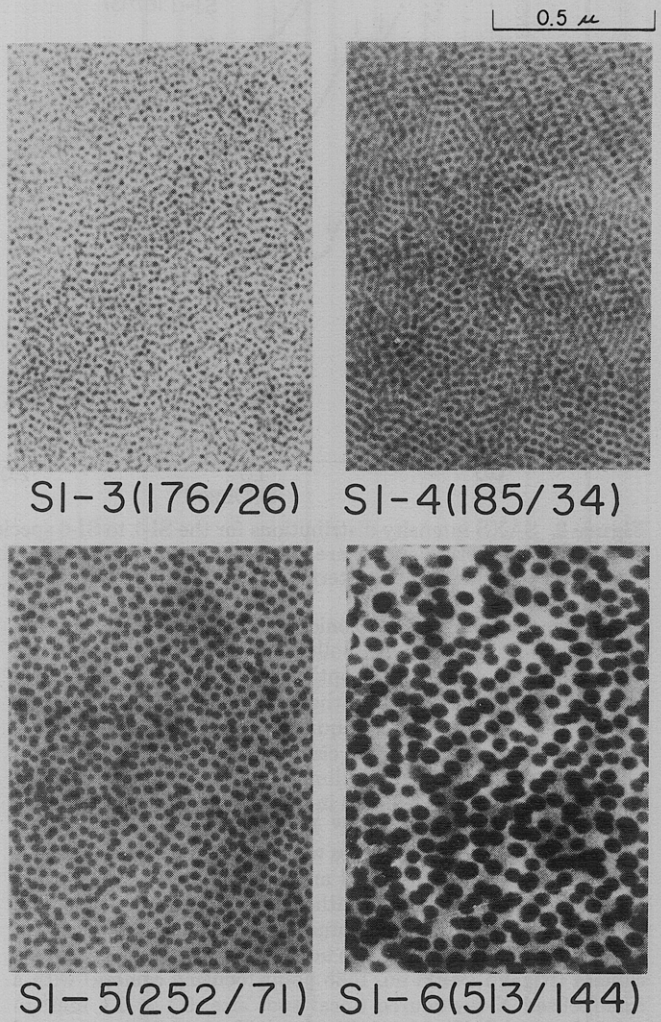

Figure 1. Typical transmission electron micrographs of the ultrathin sections stained by osmium tetraoxide for the SI-3 to SI-6 specimens. Specimens SI-1 and SI-2 also have spherical domains of polyisoprene dispersed in the matrix of polystyrene.

The film specimens used for the SAXS experiments and electron microscopic studies were prepared by casting 5% toluene solutions onto a glass plate and evaporating the solvent very gradually at 30 °C for a few days. The film specimens thus formed were further dried under vacuum (10^{-6} torr) for several days until the specimens were at constant weight.

All the film specimens of SI-1 to SI-6 thus formed have the morphology of spherical microdomains of polyisoprene dispersed in a polystyrene matrix. Some of the micrographs are shown in Figure 1. It is apparent that the size of the spheres and intersphere distance increase with increasing molecular weight.

2. SAXS Measurements. The SAXS intensity distribution was measured with a rotating-anode X-ray generator (Rigaku Denki Rotaflex RU-Z, operated at 40 kV and 200 mA). The X-ray source was monochromatized to Cu Kα radiation with a Ni filter and a pulse-height analyzer. The intensity was measured on a

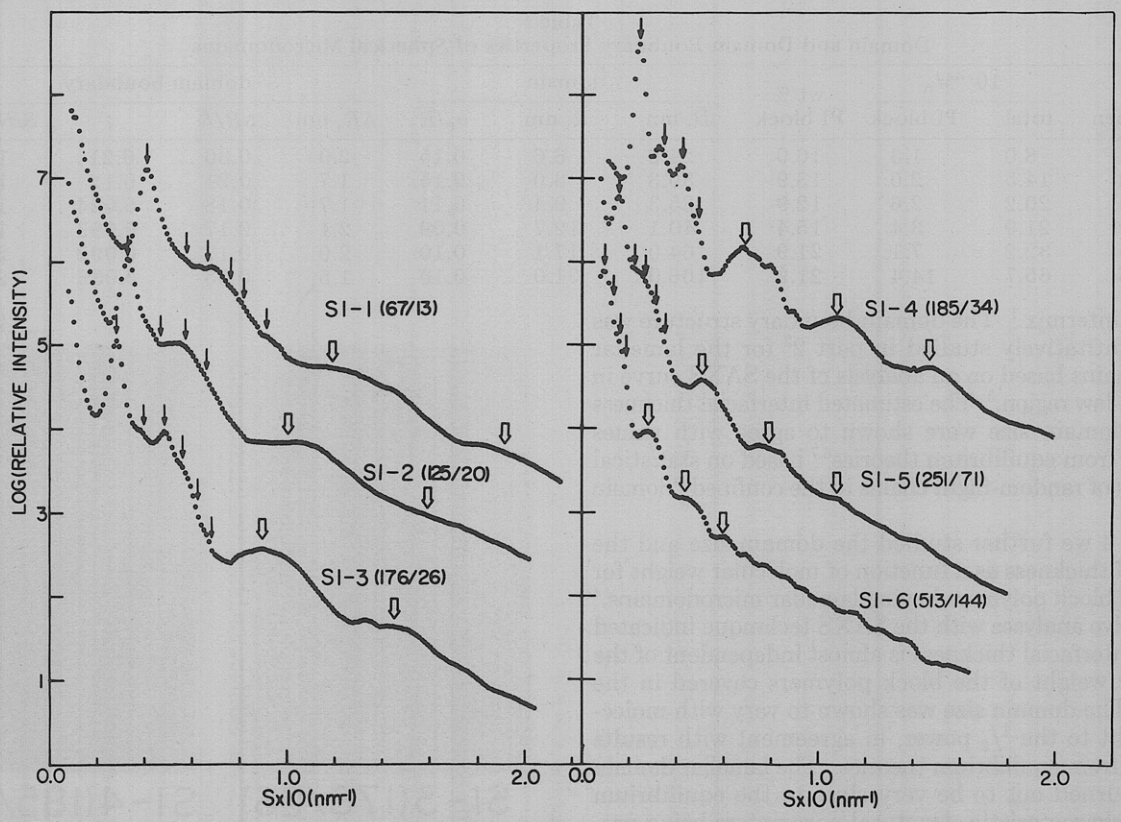

Figure 2. SAXS intensity distributions for the SI-1 to SI-6 specimens plotted against $s = (2 \sin \theta)/\lambda$, where θ is one-half the scattering angle. The scattering curves are corrected for air scattering, slit-length and slit-width smearings, and the background scattering I_b attributed to amorphous scattering from each phase.

conventional low-angle X-ray goniometer (Rigaku Denki no. 2202) with a four-slit system with Soller slits between the third and fourth slits. The setup of the optical system (focal spot size, size of the slits, distance between the slits, and the slit-length and -width weighting functions required for the slit-smearing corrections) is described in detail elsewhere.[10] The procedure, stability, and problems of the collimation correction, especially in the analyses of the SAXS data in the Porod-law region, are also described in detail elsewhere.[10] In the present analyses the intensity at large scattering angles was measured with enlarged slit widths (0.3 mm) for the third and fourth slits to gain enough counts of scattered photons without inducing any distortion of the scattering profile at the large-angle tail.

The SAXS patterns were also taken with a Huxley-Holmes-type camera (Rigaku Denki no. 1555 point-focusing camera) with a fine-focused X-ray source (focal spot size, 0.1 × 0.1 mm^2 in projection; high-brilliancy rotating-anode X-ray generator operated at 40 kV and 30 mA, Rigaku Denki). Typical SAXS patterns are shown in Figure 3.

III. Results

1. Intensity Profiles at Small Angles. Figure 2 shows the SAXS intensity distributions for the SI-1 to SI-6 specimens in the small-angle region, where the logarithm of the relative intensity is plotted against the reduced scattering angle $s = (2 \sin \theta)/\lambda$ (θ is one-half the scattering angle). The scattering curves are corrected for air scattering, absorption, and slit-length and slit-width smearings as well as for the background scattering I_b arising from local atomic order within each phase (discussed in section III-2).

Each scattering curve shows a number of scattering maxima in a manner quite different from that for the lamellar system.[2,4] With the help of electron microscopic observations we can conclude that the first scattering maximum of each scattering curve corresponds to the nearest-neighbor distance between the spherical domains ($\bar{D}$). A number of thin arrows are marked at the following

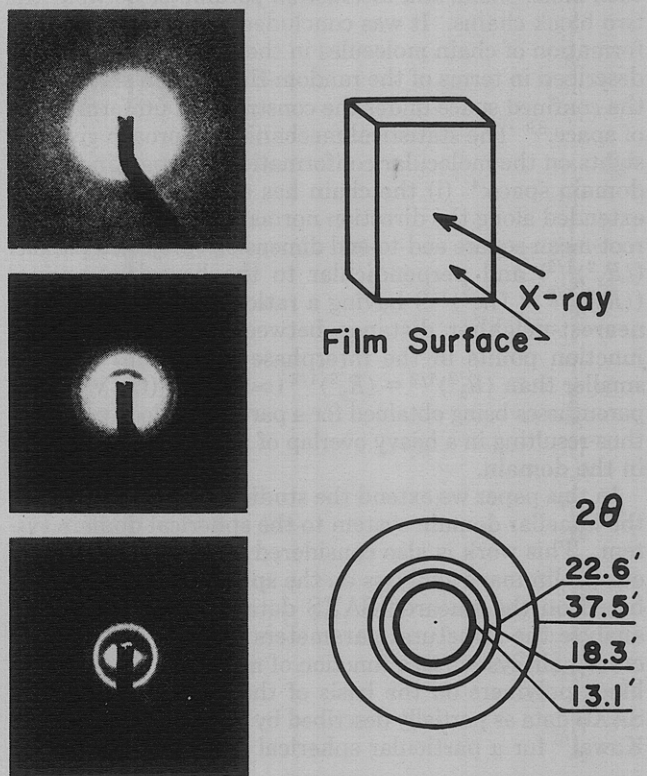

Figure 3. Typical SAXS patterns taken with mirror–monochromator optics (Huxley-Holmes camera) for the SI-4 specimen. The patterns were taken with three different exposures to show a number of scattering maxima.

scattering angles relative to the angle of the first maximum: $1:\sqrt{2}:\sqrt{3}:\sqrt{4}:\sqrt{5}:\cdots$. It is shown that the first four peaks or shoulders appear closely at the relative angular positions of $1:\sqrt{2}:\sqrt{3}:\sqrt{4}$. Thus the peaks marked by the thin ar-

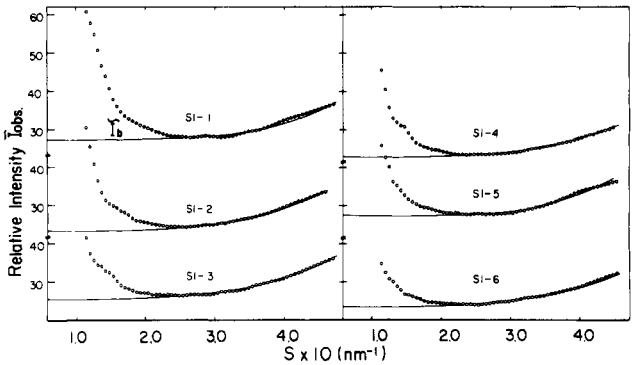

Figure 4. Relative, smeared SAXS intensity distributions in the large scattering angle region for the SI-1 to SI-6 specimens. The data are corrected for air scattering and absorption. Background scattering $\tilde{I}_b$, drawn by solid lines, was estimated from the least-squares fit of the measured curves over a sufficiently wide range ($2\theta \simeq 120$–$300'$) with the function of eq 1.

rows may arise from an interparticle interference, indicating that the spatial arrangement of the spherical domains is quite regular and may be characterized approximately by a simple cubic lattice or a cubic close pack (somewhat distorted so that the extinction rule for the perfect crystal may not be applied and that the scattering maximum is rapidly broadened with increasing order).

A number of broad scattering maxima marked by thick arrows can be concluded to be first and higher order scattering maxima from isolated spherical domains, which is again confirmed by the electron microscopic studies. Owing to the fact that the block polymers have a narrow molecular weight distribution, the distribution of the sphere size is also very narrow, giving rise to a number of intraparticle interference maxima.

Some of the scattering maxima are directly resolvable in the SAXS patterns taken with the mirror-monochromator optics (i.e., Huxley-Holmes camera), as shown in Figure 3 for the SI-4 specimen. The patterns were taken with three different exposures to show a number of scattering maxima. The most intense maximum, at $2\theta = 13.1'$, is the first-order maximum arising from an interference between nearest-neighbor particles. The maxima at $2\theta = 18.3$ and $22.6'$ are those occurring at the angular positions of $\sqrt{2}$ and $\sqrt{3}$ of the first-order maximum. The maximum corresponding to $\sqrt{4}$ is not resolvable. The broad maximum at $2\theta = 37.5'$ is the first-order scattering maximum from an isolated sphere.

2. Intensity Profiles at Large Angles. The relative smeared intensity distributions in the large scattering angle region are shown in Figure 4 for the SI-1 to SI-6 specimens. The smeared data $\tilde{I}_{obsd}$ are corrected for air scattering and absorption. The intensity increases with increasing scattering angle s, owing to an increasing contribution of amorphous scattering within each phase. This background scattering $\tilde{I}_b$ was subtracted from the measured intensity $\tilde{I}_{obsd}$ to obtain the intensity $\tilde{I}$ ($=\tilde{I}_{obsd} - \tilde{I}_b$) corrected for the background scattering. $\tilde{I}_b$ was estimated according to an empirical procedure proposed by Vonk[12] for further analyses on the domain-boundary thickness

$$\tilde{I}_b = as^n + b \tag{1}$$

where the parameters a, b, and n are determined from the least-squares fit of the measured curve over a sufficiently wide angular range ($2\theta \simeq 120$–$300'$ or $s \simeq 0.23$–0.57 nm^{-1}). Figure 4 also shows the estimated background scattering $\tilde{I}_b$ (solid lines).

In some cases the scattering curves $\tilde{I}_{obsd}$ are corrected for the slit-smearing effects, according to the procedure described in detail in a previous paper.[10] Again the desmeared intensity I_{obsd} is corrected for the background scattering I_b

$$I_b = a's^{n'} + b' \tag{2}$$

where a', b', and n' are determined in a manner similar to that used for the estimation of $\tilde{I}_b$. The scattering curves shown in Figure 2 correspond to I ($=I_{obsd} - I_b$) corrected for the background scattering.

IV. SAXS Analyses of Domain Size and Domain-Boundary Thickness

1. Interdomain Distance, Domain Size, and Interfacial Area. The scattering of X-rays from an assembly of spherical microdomains may be generally described by a paracrystalline theory of scattering.[13] If the paracrystalline macrolattice composed of regularly arranged microdomains has a random orientation, then the scattered intensity is given by[13]

$$I(s) = N[\langle f^2\rangle - \langle f\rangle^2] + (1/v)\langle f\rangle^2 Z(s) * |S(s)|^2 \tag{3}$$

where the symbol * designates a convolution operation, N is the number of particles in the assembly, v is the volume occupied by a single particle, and $f(s)$ is the scattering amplitude, given for a spherical particle of radius R by

$$f(s) = E_e(\rho_1 - \rho_2)V\Phi(U) \tag{4}$$

$$U = 2\pi Rs$$

$$V = 4\pi R^3/3$$

$$\Phi(U) = (9\pi/2)^{1/2}J_{3/2}(U)/U^{3/2} \tag{5}$$

where ρ_1 and ρ_2 are the electron density of the sphere and its surrounding medium, respectively, E_e is the scattering amplitude of a single electron, and $J_{3/2}(U)$ is the half integral order Bessel function. The function $Z(s)$ is the lattice factor of the paracrystalline macrolattice, giving rise to the interparticle interference maxima, and $S(s)$ is the shape amplitude of the assembly, contributing to the zero-order scattering.

The average nearest-neighbor distance of the sphere $\bar{D}$ was determined by using Bragg's equation

$$2\bar{D}\sin\theta_m = \lambda \tag{6}$$

where θ_m is one-half the scattering angle at which the intensity arising from the interparticle interference becomes maximum. The results are summarized in Table I. If the sphere size is monodisperse, its size R can be estimated from the scattering angle $\theta_{m,i}$ at which the scattering from the single sphere becomes maximum

$$U_{m,i} = 4\pi(R/\lambda)\sin\theta_{m,i} = 5.765, 9.10, 12.3, \ldots$$

$$\text{for } i = 1, 2, 3, \ldots \tag{7}$$

In this analysis we assume the size distribution is given by a Gaussian function $P(R)$

$$P(R) = (\text{const})\exp[-(R - \bar{R})^2/2\sigma_r^2] \tag{8}$$

Using eq 8 we calculate the average particle-scattering intensity $\langle I_p(s)\rangle$ which is then fitted with the experimental curve

$$\langle I_p(s)\rangle = \int_0^\infty dR\, P(R)f^2(s;R) \Big/ \int_0^\infty dR\, P(R) \tag{9}$$

When the sphere has a diffuse boundary rather than a sharp boundary as discussed so far, the scattering amplitude should be modified as

$$f(s) = f_0(s)\exp(-2\pi^2\sigma^2 s^2) \tag{10}$$

where $f_0(s)$ is given by eq 4 and σ is the parameter char-

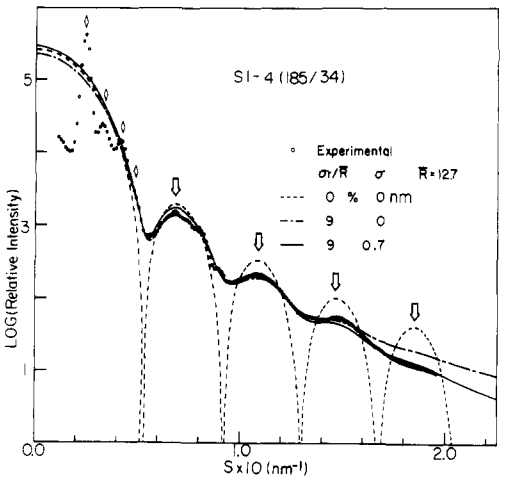

Figure 5. Measured SAXS curve for the SI-4 specimen (O) and the calculated particle scattering for an isolated sphere with monodisperse size $\bar{R}$ = 12.7 nm and $\sigma_r = \sigma = 0$ (- - -), with $\bar{R}$ = 12.7 nm, $\sigma_r/\bar{R}$ = 0.09, and σ = 0 (—·—), or with $\bar{R}$ = 12.7 nm, $\sigma_r/\bar{R}$ = 0.09, and σ = 0.7 nm (—).

acterizing the diffuseness of the boundary. The electron density profile near the boundary is given by

$$\eta(r) = \rho(r) * h(r) \tag{11}$$

and

$$h(r) = (2\pi\sigma^2)^{-3/2} \exp(-r^2/2\sigma^2) \tag{12}$$

where $\rho(r)$ is the density profile for the sphere having the sharp boundary.

Figure 5 shows a comparison between the measured scattering curve (open circles) and the calculated particle scattering for a particular spherical domain system, SI-4. The broken line is the calculated particle scattering with monodisperse size $\bar{R}$ = 12.7 nm, while the dash–dot line is the calculated curve with $\bar{R}$ = 12.7 nm and $\sigma_r/\bar{R}$ = 0.09. It is obvious that the calculated results based on the isolated particle agree better with the measured result at larger scattering angles $s \geq s_c \simeq 2.5 \times 10^{-2}$ (nm^{-1}) where the lattice factor Z approaches unity and consequently the scattering from the assembly is described in terms of independent scattering,

$$I(s) \simeq N\langle f^2 \rangle = N\langle I_p(s) \rangle \text{ (for } s > s_c) \tag{13}$$

The discrepancy between the measured and calculated results at $s < s_c$ is apparently due to a significant contribution of the interparticle interference effect.

It is also shown that the calculated result agrees better with the measured result with the introduced size distribution. However, the measured curve still deviates from the calculated curve in that the measured curve tends to drop more rapidly than the calculated one at large scattering angles $s \gtrsim 1.5 \times 10^{-1}$ (nm^{-1}). This deviation disappears when a diffuseness is introduced in the boundary of the sphere (the solid line), σ = 0.7 nm, which may be a direct indication of the diffuse boundary of the spherical domain. It should be noted that the interfacial thickness estimated this way is not free from the effect of the size distribution; i.e., one might obtain a different value of σ if one adopts a different functional form for $P(R)$. This point will be further discussed in following sections.

Figure 6 shows some results on the curve fittings between the measured (open circles) and calculated particle-scattering curves (solid lines) for SI-1 to SI-3. The average size of the sphere $\bar{R}$ and its polydispersity $\sigma_r/\bar{R}$ thus estimated are summarized in Table I. It should be noted that the size distribution $P(R)$ may be estimated in

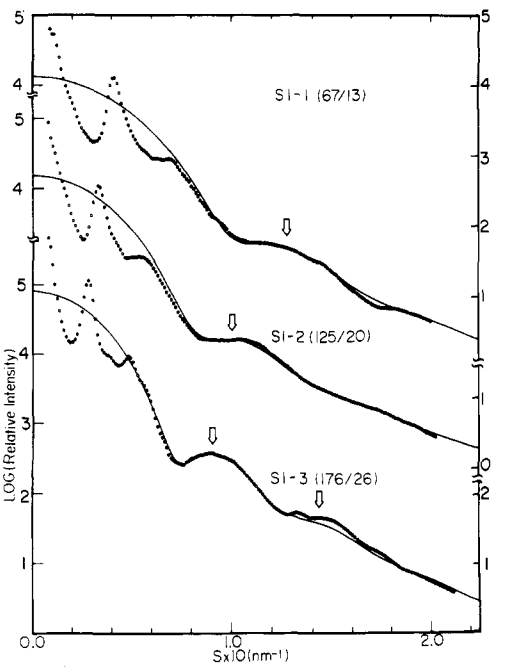

Figure 6. Typical results on the curve fittings between the measured (O) and calculated particle-scattering curves (—) with average size $\bar{R}$ and polydispersity $\sigma_r/\bar{R}$ as shown in Table I for the SI-1 to SI-3 specimens. The values of σ associated with the interfacial thickness are 0.7, 0.5, and 0.8 nm for the SI-1 to SI-3 specimens, respectively.

a more rigorous fashion by solving the integral equation of (9) for the scattering data satisfying the condition of the isolated or independent scattering. The detailed procedure is described by Fedorova and Schmidt.[14]

One can estimate an important structural parameter N (number of block polymer chains per domain) or S/N (the interfacial area occupied by a single block chain at the interface) from the estimated size of the domain, i.e., the radius of the A sphere or the interdomain distance D

$$(4\pi/3)R_A^3 = N\bar{v}_A \tag{14}$$

$$D^3/\sqrt{2} = N(\bar{v}_A + \bar{v}_B) \tag{15}$$

or

$$S/N = 3\bar{v}_A/R_A \tag{16}$$

where $\bar{v}_A$ is the molecular volume of an A-block chain and eq 15 is derived for hexagonal close packing. The quantity S/N thus evaluated from eq 16 is summarized in Table I.

2. Domain-Boundary Interphase. A. Full Analysis Based on Desmeared Data. It is well-known that the scattering intensity at large scattering angles for an isotropic pseudo-two-phase system is asymptotically given by[15]

$$I(s) = (2\pi)^{-3} I_e(\rho_1 - \rho_2)^2 A_{int} s^{-4} \exp(-4\pi^2\sigma^2 s^2) \tag{17}$$

where I_e is the Thomson scattering from an electron, A_{int} is the total interfacial area of the system, and σ is the parameter characterizing the interfacial thickness as defined in eq 12. The intensity $I(s)$ is, of course, corrected for the background scattering I_b. When σ = 0, the function $h(r)$ approaches the δ function and therefore the electron density variation becomes typical of the ideal two-phase system having a stepwise transition of the density at the interface. For such an ideal two-phase system, the intensity $I(s)$ is proportional to s^{-4} (Porod's rule).[5,16]

From eq 17 one can estimate the parameter σ related to the interfacial thickness from the slope of the plot ln

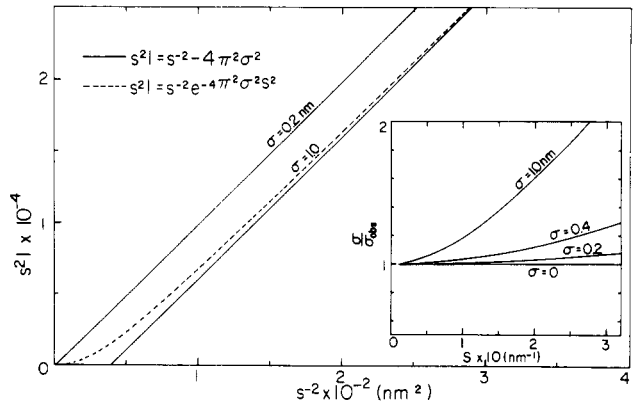

Figure 7. Plot of $s^2I(s)$ vs. s^{-2} on the basis of the narrow-interphase approximation (eq 24) (—) and of the rigorous eq (17) (- - -). When σ is small (e.g., σ = 0.2 nm), the two plots become identical, yielding a correct value of σ for all s values. When σ becomes large (e.g., σ = 1.0 nm), the two plots start to diverge; the apparent value of σ estimated on the basis of eq 24 (defined as σ_{obsd}) depends on s at which the straight line is drawn. The larger the value s, the poorer the approximation, giving rise to a smaller apparent value of σ_{obsd} and a σ/σ_{obsd} ratio larger than unity.

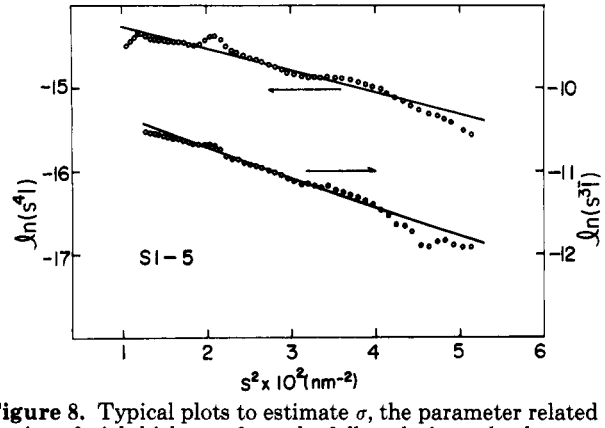

Figure 8. Typical plots to estimate σ, the parameter related to the interfacial thickness, from the full analysis on the desmeared data (ln $[s^4I(s)]$ vs. s^2) and on the smeared data (ln $[s^3\tilde{I}(s)]$ vs. s^2). SI-5 specimen.

$[s^4I(s)]$ vs. s^2 (see, for example, Figure 8). Although this full analysis involves no assumption other than the Gaussian smoothing function for $h(r)$ and is most straightforward, it has a demerit that one has to work on the desmeared scattering curves. Desmearing at the large scattering angle tail is not always warranted due to the severe amplification of the statistical errors in the photon counting. In our previous paper[10] we showed that one may obtain reliable desmeared intensity data in the large-angle tail by reducing the width of the slit-length weighting function with the Soller slits. It is obvious from the nature of the integral equation, a Fredholm integral equation of the first kind (see eq 18), that the wider the width of the weighting function, the more severe the amplification of the statistical errors in the data. The reduction of the scattering power due to the insertion of the Soller slits was overcome by using a high-flux X-ray source (12-kW rotating-anode generator) and prolonged counting time.

It is important to comment on the effects of waviness of the interface and of size distributions of the domain on estimated interfacial thickness. In principle this surface waviness and size distribution do not affect the interfacial thickness estimated by the analyses on the systematic deviation of the SAXS curve at the large-angle tail from Porod's rule, if the wavelength of the surface waviness is much larger than the interfacial thickness or if the size distribution of the domains is narrow enough so that the domains having their sizes comparable to the interfacial thickness do not contribute to the scattering. These conditions are usually satisfied in block polymers such as we are discussing here. Generally the surface waviness and the size distribution affect the total interfacial area A_{int} in eq 17 and push the Porod-law region toward higher scattering angles.

Table II
Comparison of Domain-Boundary Thickness (nm) Estimated with Various Methods

ΔR_∞ [a]	ΔR_{narrow} [b]	ΔR_{FD} [c]	ΔR_{FS} [d]
1.1 ± 0.1	1.4 ± 0.2	1.7 ± 0.2	1.7 ± 0.2

[a] Values obtained with the infinite slit-height and narrow-interphase approximations; $s\tilde{I}$ vs. s^{-2}. [b] Values obtained with the narrow-interphase approximation; s^2I vs. s^{-2}. [c] Values obtained from the desmeared curves with the full analysis; ln (s^4I) vs. s^2. [c] Values obtained from a new analysis based on the full analysis of the smeared curve (a nonlinear curve fitting); ln $(s^3\tilde{I})$ vs. s^2.

B. Full Analysis Based on Smeared Data. A New Technique. We propose here a full analysis based on smeared data for cases when the desmearing of the scattering curve at the tail region involves great difficulty. The smeared intensity $\tilde{I}(s)$ and the desmeared intensity $I(s)$ are related by the integral equation

$$\tilde{I}(s) = \int_{-\infty}^{\infty} du\ W_l(u) I([s^2 + u^2]^{1/2}) \qquad (18)$$

where $W_l(u)$ is the slit-length weighting function and $W_w(u)$, the slit-width weighting function, is assumed to be narrow enough to involve no smearing effect on the scattering data under consideration (this condition is usually satisfied). In principle one can substitute eq 17 into eq 18 to obtain the smeared theoretical scattering curve, $\tilde{I}_{theor}(s)$, for a given σ. Then one can estimate σ by a nonlinear curve fitting between $\tilde{I}_{theor}(s)$ and $\tilde{I}$, measured intensity.

When the weighting function is approximated by a Gaussian function

$$W_l(u) = W_l(0) \exp(-p^2u^2) \qquad (19)$$

one can obtain an analytical expression for $\tilde{I}_{theor}(s)$ (see Appendix)

$$\tilde{I}_{theor}(s) = Cs^{-3}\{[1 - 2s^2(p^2 + 4\pi^2\sigma^2)] \times \mathrm{Erfc}\,[s(p^2 + 4\pi^2\sigma^2)^{1/2}] \exp(s^2p^2) + s(p^2 + 4\pi^2\sigma^2)^{1/2} \exp(-4\pi^2\sigma^2s^2)\} \qquad (20)$$

where

$$\mathrm{Erfc}\,(x) = \int_x^{\infty} dt \exp(-t^2)$$

and

$$C = (2\pi)^{-3}\pi^{1/2}I_e(\rho_1 - \rho_2)^2W_l(0)A_{int} \qquad (21)$$

Equation 20 is a generalized form of the equation derived by Ruland[15] for the case of $p = 0$, i.e., the case of infinite slit height. Thus one can estimate σ from a nonlinear curve fitting of the smeared data [in the plot of ln $(s^3\tilde{I})$ vs. s^2] and the smeared theoretical intensity $\tilde{I}_{theor}$ [in the plot of ln $(s^3\tilde{I}_{theor})$ vs. s^2] with least-squares methods. In Figure 8 is included a typical result of the nonlinear curve fitting, where the experimental and theoretical data are shown by open circles and a solid curve, respectively.

Good agreement is obtained between the σ values estimated from the desmeared and smeared data (see Table II). Table I summarizes the result on the interfacial

thickness estimated by the full analysis of the smeared data. It should be noted that the value σ is converted to the thickness $\Delta R = (2\pi)^{1/2}\sigma$, as will be described later.

An overall volume fraction of the interphase f was estimated from the measured $\bar{R}$ and ΔR by using the relationship

$$f = 2\beta(\beta^2 + 12)\phi_{PI}/[(2 - \beta)^3 + 2\phi_{PI}\beta(\beta^2 + 12)] \quad (22)$$

where

$$\beta = \Delta R/R \quad (23)$$

and ϕ_{PI} is the volume fraction of polyisoprene chain.

C. Remarks on the Narrow-Interphase Approximation and the Infinite Slit-Height Approximation. In the context of the narrow-interphase approximation, σ is so small that a series expansion of the exponential term in eq 17 is truncated at the second term

$$I(s) = (\text{const})s^{-4}[1 - 4\pi^2\sigma^2 s^2] \quad (24)$$

Thus in this case the plot of $s^2I(s)$ vs. s^{-2} yields the value σ from the slope and intercept at $s^{-2} = 0$. In reality this approximation is not necessarily valid, especially when the analyses involve the scattered intensity at large s. In our previous paper[10] we pointed out that the analyses based upon the narrow-interphase approximation yield a thinner interphase than the full analyses.

The experimental observations as discussed above can be theoretically verified as shown in Figure 7, where $s^2I(s)$ are plotted against s^{-2} on the basis of eq 24 (solid line, narrow-interphase approximation) and of eq 17 (broken line, rigorous equation). When σ is very small (e.g., σ = 0.2 nm), the plots based on the approximated and rigorous equations become identical, yielding a correct value of σ for all s values. On the other hand, when σ becomes large (e.g., σ = 1.0 nm), the two plots start to diverge as shown in the figure, and the apparent value of σ estimated on the basis of eq 24 (defined as σ_{obsd}) depends on s at which the straight line is drawn. The larger the value of s, the poorer the approximation, giving rise to the smaller apparent value of σ_{obsd}. The figure also shows the ratio of the true value of σ to the apparent value σ_{obsd} as a function of the scattering angle s. It is clearly seen that the approximation results in a smaller estimation of the interphase and that the errors involved by using the approximation increase with increasing interfacial thickness. Essentially an identical conclusion was obtained by Koberstein, Morra, and Stein.[17]

If the slit-height is infinite (i.e., $p = 0$ in eq 19) and the narrow-interphase approximation is still valid, then eq 20 results in

$$\tilde{I}(s) = (\text{const})s^{-3}(1 - 8\pi^2\sigma^2 s^2) \quad (25)$$

Then the plot of $s\tilde{I}(s)$ vs. s^{-2} gives the values σ. The analysis based on the infinite slit-height approximation gives a much smaller value of the interphase than the value based on the full analysis, as shown in Table II. The errors, of course, depend on the accuracy of the approximation. This approximation is generally poor in the tail angle region. Table II summarizes a comparison of the domain-boundary thickness estimated from the various methods discussed in this paper, where σ is converted to $\Delta R = (2\pi)^{1/2}\sigma$.

D. New Definition of the Interfacial Thickness ΔR Corresponding to the Linear Density Profile. The scattering intensity from spheres having a linear electron density variation at the interface is shown to be given,[3] at large scattering angles, by

$$I(s) = (\text{const})s^{-4}[1 - (\pi^2\Delta R^2/3)s^2 + \mathcal{O}(s^4)] \quad (26)$$

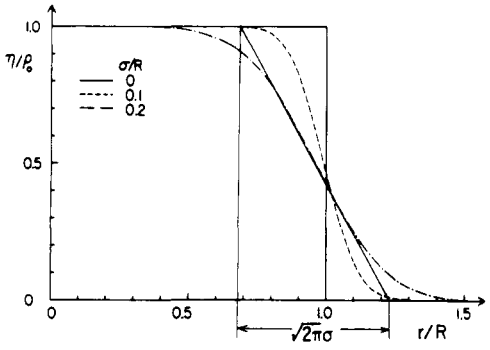

Figure 9. Sigmoidal electron density variation in the radial direction of the sphere as expected from eq 11 and 12, or eq 29, and the definition of $\Delta R = (2\pi)^{1/2}\sigma$, the interfacial thickness corresponding to the linear density transition.

where ΔR is the interfacial thickness. In our previous paper[10] σ is interrelated to the linear interfacial thickness ΔR based on the narrow-interphase approximation, i.e., by comparing eq 24 and 26

$$\Delta R = 12^{1/2}\sigma \quad (27)$$

Since the narrow-interphase approximation is not generally valid, we shall define ΔR in a more general fashion

$$\Delta R \equiv \rho_0/|\mathrm{d}\eta(r)/\mathrm{d}r|_{r=R} \quad (28)$$

where from eq 11 and 12, $\eta(r)$ near the interface is given by

$$\eta(r) = \rho_0\pi^{-1/2}\left\{\mathrm{Erf}\left(\frac{r+R}{\sqrt{2}\sigma}\right) + \frac{\sigma}{\sqrt{2}r}\exp\left[-\left(\frac{r+R}{\sqrt{2}\sigma}\right)^2\right] - \mathrm{Erf}\left(\frac{r-R}{\sqrt{2}\sigma}\right) + \frac{\sigma}{\sqrt{2}r}\exp\left[-\left(\frac{r-R}{\sqrt{2}\sigma}\right)^2\right]\right\} \quad (29)$$

From eq 28 and 29, it follows for small σ that

$$\Delta R \simeq (2\pi)^{1/2}\sigma \quad (30)$$

The same relationship as eq 30 can be used for other domain morphology. Figure 9 shows the sigmoidal electron density profile obtained from eq 29 and the linear density profile as defined by eq 30. The new definition gives a smaller value of ΔR than the old definition by about 40%.

V. Comparison with Equilibrium Theories and Discussion

1. Theories and Parameters. We calculated equilibrium values for the radius of the spherical domain R, interdomain distance D, and the interfacial thickness ΔR (as defined by eq 28) based upon the theory of spherical microdomains developed by Helfand and Wasserman.[18] The formula for the AB diblock polymer is used.

The parameters required for the calculations of the equilibrium values are the statistical segment lengths (b_K), the number density of monomeric units in homopolymers (ρ_{0K}), and the interaction parameter α between A and B polymers.

As for the statistical segment length of polystyrene (b_{PS}) we used the value reported by Ballard, Wignall, and Schelten[19] from neutron scattering experiments for bulk polystyrene

$$b_{PS} = [\langle R_{PS}^2\rangle_0/\bar{Z}_{PS}]^{1/2} = 0.68 \text{ (nm)} \quad (31)$$

where $\langle R^2\rangle_0^{1/2}$ is the unperturbed chain dimension, and $\bar{Z}$ is the degree of polymerization. For polyisoprene having

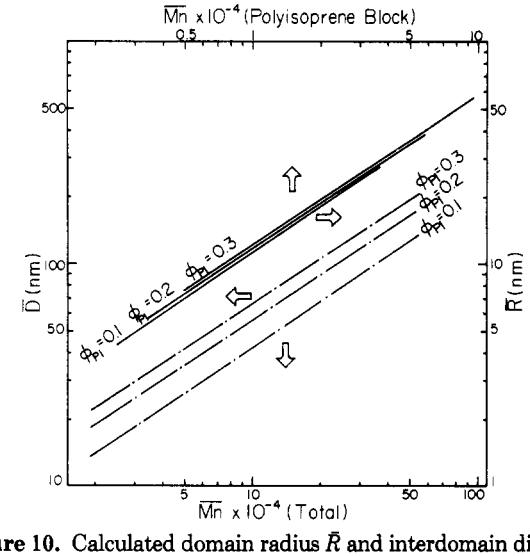

Figure 10. Calculated domain radius $\bar{R}$ and interdomain distance $\bar{D}$ as a function of the molecular weight of the block chain (polyisoprene) forming the spherical domain and that of the entire diblock polymer (styrene–isoprene), respectively. The calculations were performed on the basis of Helfand–Wasserman theory for the block polymers having 10, 20, and 30 wt % polyisoprene.

the particular microstructure as described earlier, we measured[11]

$$b_{PI} = 0.59 \text{ (nm)} \tag{32}$$

The densities of pure polymers were measured by a density gradient tube method

$$\rho_{0PS} = 1.01 \times 10^4 \text{ (mol/m}^3\text{)}$$

$$\rho_{0PI} = 1.36 \times 10^4 \text{ (mol/m}^3\text{)} \tag{33}$$

As for the interaction parameter α, we adopted a value at 20 °C according to the formula obtained by Rounds and McIntyre as cited by Helfand[9]

$$\alpha = (\delta_A - \delta_B)^2/RT = -900 + 7.5 \times 10^5/T \text{ (mol/m}^3\text{)} \tag{34}$$

where δ_A is the solubility parameter of the A-block chain. It should be noted that this result was obtained for polystyrene and *cis*-1,4-polyisoprene and is therefore not strictly applicable to the interaction with polyisoprene having a high vinyl content.

Figure 10 shows the calculated domain size $\bar{R}$ and interdomain distance $\bar{D}$ as a function of the molecular weight of the block chain (polyisoprene block) forming the spherical domains and total molecular weight of the styrene–isoprene diblock polymers, respectively. The calculations were performed for the block polymers having 10, 20, and 30 wt % polyisoprene. The calculated values of $\bar{R}$ and $\bar{D}$ are different for the different chemical compositions of the block polymers, due to asymmetry in the statistical segment lengths and densities for the two corresponding homopolymers. The calculated results indicate that for $\phi_{PI} = 0.2$

$$D \simeq 0.025M_t^{2/3}$$

$$R_A \simeq 0.025M_A^{2/3} \tag{35}$$

in units of nanometers in the molecular weight range covered in this work, where M_t is the total molecular weight of the diblock polymer and M_A is the molecular weight of the A-block chain forming the spherical domain.

2. Comparison with Experimental Results. In Tables III and IV are shown comparisons of the measured and predicted domain properties (D and R) and the domain-boundary properties (ΔR and $\Delta R/R$) for the series of the styrene–isoprene block polymers.

Table III
Comparison of Measured and Predicted Domain Properties of the Spherical Domain System of Styrene-Isoprene Block Copolymers

specimen	$10^{-3}\overline{M}_n$ PS/PI	D, nm		R, nm	
		exptl	calcd[a]	exptl	calcd[a]
SI-1	67/13	24.2 ± 0.2	45	7.4 ± 0.1	14.1
SI-2	125/20	30.3 ± 0.3	63	8.5 ± 0.1	18.6
SI-3	176/26	35.3 ± 0.5	76	9.6 ± 0.1	22.1
SI-4	185/34	40.1 ± 0.5	87	13.0 ± 0.2	26.7
SI-5	251/71	64.0 ± 1.0	129	18.0 ± 0.2	44.4
SI-6	513/144	106.0 ± 4.0	205	33.0 ± 0.4	70.5

[a] Helfand, E.; Wasserman, Z. R. *Macromolecules* 1978, *11*, 960.

Table IV
Comparison of Measured and Predicted Domain-Boundary Thicknesses of Spherical Domain Systems

specimen	$10^{-3}\overline{M}_n$ PS/PI	ΔR, nm		$\Delta R/R$		
		exptl	calcd[a]	exptl	H[a]	M[b]
SI-1	67/13	2.0 ± 0.1	1.3	0.30	0.09	0.20
SI-2	125/20	1.7 ± 0.1	1.3	0.21	0.07	0.12
SI-3	176/26	1.7 ± 0.2	1.3	0.18	0.06	0.10
SI-4	185/34	2.1 ± 0.2	1.3	0.17	0.05	0.08
SI-5	251/71	2.0 ± 0.1	1.3	0.12	0.03	0.03
SI-6	513/144	1.5 ± 0.2	1.3	0.048	0.02	0.02

[a] Helfand, E.; Wasserman, Z. R. *Macromolecules* 1978, *11*, 960. [b] Meier, D. J. In "Block and Graft Copolymers"; Burke, J. J., Weiss, V.; Eds.; Syracuse University Press: Syracuse, N.Y., 1973.

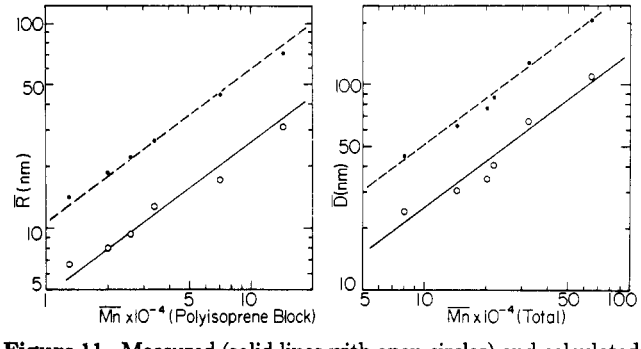

Figure 11. Measured (solid lines with open circles) and calculated (broken lines with solid circles) $\bar{R}$ and $\bar{D}$ as a function of molecular weight of the block polymers.

It is at first striking that the experimental values for the radii $\bar{R}$ and interdomain distances $\bar{D}$ are found to be much less than the equilibrium values (almost $^1/_2$ of the theoretical values) but that the relative molecular weight dependencies of the measured and predicted values are yet very close to each other. The latter tendency is more clearly observed in Figure 11 in which the predicted and measured results are shown, respectively, by broken lines with solid circles and by solid lines with open circles. The scattering of the data points around the solid line arises from variation of the chemical composition of the block polymers. Thus the measured $\bar{R}$ and $\bar{D}$ also are shown to follow the $^2/_3$ power law in terms of their molecular weight dependencies.

These tendencies observed for the spherical domain system are quite different from those observed for the lamellar domain systems, in which one finds almost complete agreement between the theoretical and experimental results in terms of both the absolute values and the relative molecular weight dependencies.[4] The relative molecular

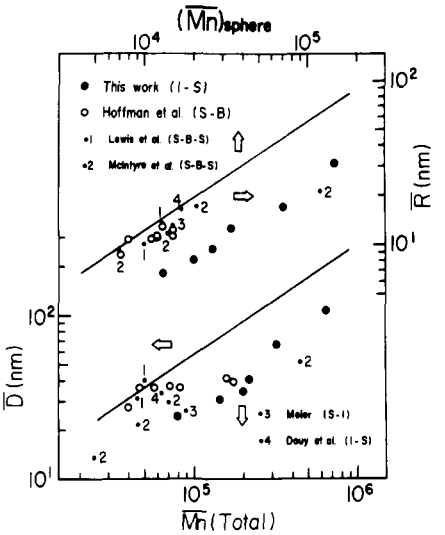

Figure 12. Measured $\bar{R}$ and $\bar{D}$ as a function of molecular weight of the block polymer for styrene–isoprene (S–I) and styrene–butadiene (S–B) diblock polymers and styrene–butadiene–styrene (S–B–S) triblock polymers. The first letter S of S–B, S–B–S, and S–I or I of I–S designates the block chain forming the spherical domains. The solid lines are calculated from the theory of Helfand and Wasserman for the block polymers having 20 wt % polyisoprene or polybutadiene. Polybutadiene is assumed to have the same parameters as polyisoprene. $(\bar{M}_n)_{sphere}$ designates the molecular weight of the block sequence which forms the spherical domain.

weight dependence of the domain size (i.e., $^2/_3$ power law) is identical with that observed for the lamellar domain system.[4] These results will be further discussed in the next section in relation to equilibrium and nonequilibrium aspects of the spherical domain system.

The calculated interfacial thickness (1.3 nm) is independent of the molecular weight, which is a consequence of the narrow-interphase approximation in the theory.[7,9,18] It should be noted that the theory of Helfand and Wasserman[18] invokes also the assumption of localized energetic interaction. The nonlocality of the interaction[20,21] is shown in the previous paper[4] to hardly affect the domain size and the interfacial thickness (the interfacial thickness being slightly thicker by involving the nonlocal interaction). The measured interfacial thickness is shown to be about 1.8 nm, almost independent of the molecular weight of the block polymers over the molecular weight range covered in this work, and to be in good agreement with the calculated results. The discrepancy between the measured and calculated values should be within the errors involved in determining the interaction parameter α.

3. Discussion. Equilibrium and Nonequilibrium Aspects of the Spherical Domain Systems. In the preceding section the observed domain sizes ($\bar{R}$ or $\bar{D}$) are shown to be much smaller than the equilibrium values. This observation may be further confirmed by the results shown in Figure 12, where $\bar{R}$ and $\bar{D}$ are plotted as a function of the molecular weight of the block polymer for styrene–isoprene (S–I) and styrene–butadiene (S–B) diblock polymers and styrene–butadiene–styrene (S–B–S) triblock polymers. The first letter S of S–B, S–B–S, and S–I or I of I–S designates the block chain forming the spherical domains. In the figure are included our data (shown in Table I) (large solid circles) as well as data by Hoffmann and co-workers[22] (large open circles), Lewis and Price[23] (small solid circles numbered 1), McIntyre and co-workers[24] (small solid circles numbered 2), Meier[25] (small solid circles numbered 3), and Douy and co-workers[26] (small solid circles numbered 4). The solid lines are calculated from the theory of Helfand and Wasserman[18] for the same set of the parameters as described in section V-1 for the block polymers having 20 wt % polyisoprene or polybutadiene. Polybutadiene is assumed to have the same parameters as polyisoprene.

Although the data points are somewhat scattered, primarily due to variation of the chemical composition, microstructure of the block polymers, and film-preparing conditions, a general trend is that the observed values are generally much smaller than the calculated values. Only those polymers which have very low molecular weight and high polyisoprene or polybutadiene content closely follow the predicted behavior.

This discrepancy in the absolute domain size may be attributed to a nonequilibrium effect encountered during the solvent evaporation process. During the solvent evaporation, the system attains a new equilibrium by changing the domain size, i.e., by changing the number N of block polymer chains per spherical domain. The lamellar or cylindrical domains can change their sizes or the number N simply by shrinking along the interface, i.e., by decreasing the distance between adjacent chemical junction points along the interface. On the other hand, the spherical domain can change its size only by a process involving transport of A(B) chains through the matrix of B(A) chains. This process must overcome a larger energetic barrier than that involved in the lamellar or cylindrical domains. This must be the main reason that the nonequilibrium effect of the spherical domain system is large compared with that of the lamellar system reported in previous work.[4]

The energetic barrier increases with increasing concentration for a given solvent–polymer combination and the molecular weight of the block polymer. Consequently the domain morphology (i.e., the value N) is fixed at a certain concentration. Thus the observed values of $\bar{D}$ and $\bar{R}$ in the solid state may reflect the equilibrium values at some concentrations but not at 100% polymer, giving rise to the relative molecular weight dependencies of $\bar{R}$ and $\bar{D}$ close to those predicted from the equilibrium theory.[18]

The radius R_A, interdomain distance D, and interfacial area occupied by a block chain S/N are related to the molecular volume $\bar{v}_A$ and $\bar{v}_B$ as in eq 14–16. A possible interpretation of the discrepancy of the absolute values of D and R_A may be made in terms of the nonequilibrium effect on the number N; i.e., the number N in the real system is much smaller than the equilibrium value. This nonequilibrium effect on N makes the size of the domain R_A and the interdomain distance D smaller by the same fraction, the tendency of which is exactly identical with that found in our experimental results (see Table III or Figure 11).

The real spherical domain systems in the solid state are therefore generally in a metastable state, having excess interfacial area S/N, interfacial volume, and, consequently, excess free energy in comparison with the equilibrium domain system. These conclusions are confirmed by the results shown in Figures 13 and 14, where the interfacial area per block chain S/N and the interfacial volume fraction f for the spherical domain systems are compared with those for the lamellar domain system which closely follows equilibrium, as clarified in the previous paper.[4] The interfacial area S/N for both spherical and lamellar microdomain systems is shown to have a relative molecular weight dependence as described by the $^1/_3$ power law, which may be verified from eq 16 and 35. Although the size of the spherical domain in the real system is much smaller than the equilibrium size due to the nonequilib-

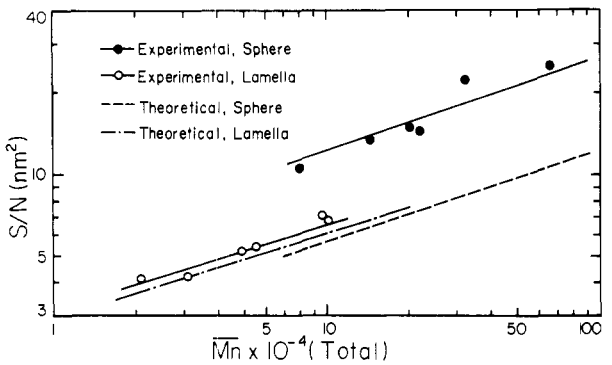

Figure 13. Measured and calculated interfacial area S/N for the spherical and lamellar microdomains as a function of total molecular weight of the S–I diblock polymers.

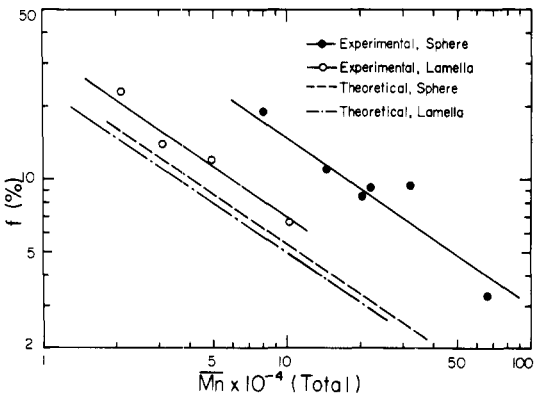

Figure 14. Measured and calculated interfacial volume fraction f for the spherical and lamellar microdomains as a function of total molecular weight of the S–I diblock polymers.

rium effect, as discussed in this section, the molecular conformation in the spherical domain and also in the matrix is expected to be close to that in the equilibrium state, as may be clarified from the fact that the relative molecular weight dependencies of $\bar{R}$ and $\bar{D}$ are close to those expected from the equilibrium theory.

Acknowledgment. This work was supported in part by a Grant-in-Aid for Scientific Research from the Ministry of Education, Japan (243021), and by a scientific research grant from the Japan Synthetic Rubber Co., Ltd., Tokyo, Japan, and the Bridgestone Tire Co., Ltd., Tokyo, Japan.

Appendix. Derivation of Equation 20

From eq 17–19, it follows that

$$\tilde{I}_{\text{theor}}(s) = I_e[W_1(0)(\rho_1 - \rho_2)^2 A_{\text{int}}/4\pi^3]Q \exp(-4\pi^2\sigma^2 s^2) \quad \text{(A-1)}$$

where

$$Q = \int_0^\infty du\ (s^2 + u^2)^{-2} \exp[-(p^2 + 4\pi^2\sigma^2)u^2] \quad \text{(A-2)}$$

Equation A-2 may be solved by using Parseval's theorem, i.e.

$$\int_0^\infty dy\ F_c(y)G_c(y) = \int_0^\infty du\ f(u)g(u) \quad \text{(A-3)}$$

where

$$F_c(y) = (2/\pi)^{1/2} \int_0^\infty du\ f(u) \cos(uy) \quad \text{(A-4)}$$

$$G_c(y) = (2/\pi)^{1/2} \int_0^\infty du\ g(u) \cos(uy) \quad \text{(A-5)}$$

If $f(u)$ and $g(u)$ are defined as

$$f(u) = (s^2 + u^2)^{-2} \quad \text{(A-6)}$$

$$g(u) = \exp[-(p^2 + 4\pi^2\sigma^2)u^2] \quad \text{(A-7)}$$

then

$$F_c(y) = (\pi/8)^{1/2} \frac{1 + sy}{s^3} \exp(-sy) \quad \text{(A-8)}$$

$$G_c(y) = [2(p^2 + 4\pi^2\sigma^2)]^{-1/2} \exp[-y^2/4(p^2 + 4\pi^2\sigma^2)] \quad \text{(A-9)}$$

From eq A-2, A-3, and A-6 to A-9, it follows that

$$Q = \int_0^\infty du\ f(u)g(u) = \int_0^\infty dy\ F_c(y)G_c(y)$$

$$= (\pi/4)^{1/2} s^{-3}\{[1 - 2s^2(p^2 + 4\pi^2\sigma^2)] \times \text{Erfc}\ [s(p^2 + 4\pi^2\sigma^2)^{1/2}] \exp[s^2(p^2 + 4\pi^2\sigma^2)] + s(p^2 + 4\pi^2\sigma^2)^{1/2}\} \quad \text{(A-10)}$$

Equation 20 is obtained from eq A-1, A-2, and A-10.

References and Notes

(1) Hashimoto, T.; Nagatoshi, K.; Todo, A.; Hasegawa, H.; Kawai, H. *Macromolecules* **1974**, *7*, 364.
(2) Hashimoto, T.; Todo, A.; Itoi, H.; Kawai, H. *Macromolecules* **1977**, *10*, 377.
(3) Todo, A.; Uno, H.; Miyoshi, K.; Hashimoto, T.; Kawai, H. *Polym. Eng. Sci.* **1977**, *17*, 587.
(4) Hashimoto, T.; Shibayama, M.; Kawai, H. *Macromolecules* **1980**, *13*, 1237.
(5) Porod, G. *Kolloid Z. Z. Polym.* **1951**, *124*(2), 83; **1952**, *125*(1), 51; **1952**, *125*(2), 108.
(6) Meier, D. J. *Prepr., Polym. Colloq., Soc. Polym. Sci. Jpn., Kyoto* **1977**, 83.
(7) Helfand, E.; Wasserman, Z. R. *Macromolecules* **1976**, *9*, 879.
(8) Meier, D. J. *J. Polym. Sci., Part C* **1969**, *26*, 81.
(9) Helfand, E. *Macromolecules* **1975**, *8*, 552.
(10) Todo, A.; Hashimoto, T.; Kawai, H. *J. Appl. Crystallogr.* **1978**, *11*, 558.
(11) Hashimoto, T.; Nakamura, N.; Shibayama, M.; Izumi, A.; Kawai, H. *J. Macromol. Sci.—Phys.* **1980**, *B17*(3), 389.
(12) Vonk, C. G. *J. Appl. Crystallogr.* **1973**, *6*, 81.
(13) Hosemann, R.; Bagchi, S. N. "Direct Analysis of Diffraction by Matter"; North-Holland Publishing Co.: Amsterdam, 1962.
(14) Fedorova, I. S.; Schmidt, P. W. *J. Appl. Crystallogr.* **1978**, *11*, 405.
(15) Ruland, W. *J. Appl. Crystallogr.* **1971**, *4*, 70.
(16) Debye, P.; Anderson, H. R., Jr.; Brumberger, H. *J. Appl. Phys.* **1957**, *28*, 679.
(17) Koberstein, J.; Morra, B.; Stein, R. S. *J. Appl. Crystallogr.* **1980**, *13*, 34.
(18) Helfand, E.; Wasserman, Z. R. *Macromolecules* **1978**, *11*, 960.
(19) Ballard, D. G. H.; Wignall, G. D.; Schelten, J. *Eur. Polym. J.* **1973**, *9*, 965.
(20) Helfand, E.; Tagami, Y. *J. Chem. Phys.* **1975**, *56*, 3592.
(21) Helfand, E.; Sapse, A. M. *J. Chem. Phys.* **1975**, *62*, 1327.
(22) Hoffmann, M.; Kämpf, G.; Krömer, H.; Pampus, G. *Adv. Chem. Ser.* **1971**, *No. 99*, 351.
(23) Lewis, P. R.; Price, C. *Polymer* **1972**, *12*, 258.
(24) Campos-Lopez, E.; McIntyre, D.; Fetters, L. J. *Macromolecules* **1973**, *6*, 415.
(25) Meier, D. J. In "Block and Graft Copolymers"; Burke, J. J., Weiss, V., Eds.; Syracuse University Press: Syracuse, N.Y., 1973.
(26) Douy, A.; Mayer, R.; Rossi, J.; Gallot, B. *Mol. Cryst. Liq. Cryst.* **1969**, *7*, 103.